ELSEVIER

Journal of Hazardous Materials 142 (2007) 130–137

Journal of Hazardous Materials

www.elsevier.com/locate/jhazmat

Photocatalytic degradation of methyl red by TiO_2: Comparison of the efficiency of immobilized nanoparticles versus conventional suspended catalyst

G. Mascolo [a,*], R. Comparelli [b], M.L. Curri [b], G. Lovecchio [a], A. Lopez [a], A. Agostiano [b,c]

[a] *Istituto di Ricerca Sulle Acque, Consiglio Nazionale delle Ricerche, Via F. De Blasio 5, I-70123 Bari, Italy*
[b] *CNR IPCF, Bari Division c/o Dip. di Chimica, Università di Bari, via Orabona 4, I-70126 Bari, Italy*
[c] *Dipartimento di Chimica, Università di Bari, via Orabona 4, I-70126 Bari, Italy*

Received 12 May 2006; received in revised form 22 June 2006; accepted 30 July 2006
Available online 3 August 2006

Abstract

The photocatalytic efficiency of supported TiO_2 nanoparticles (mean size 6 nm), immobilized onto the inner walls of a cylindrical glass photoreactor was compared versus the performance of conventional TiO_2 Degussa P25 catalyst. For this purpose the degradation of methyl red dye was used as evaluation test. The obtained results showed that the TiO_2 Degussa P25 catalyst is more efficient than the supported nanoparticles. The poorer performance of the nanosized catalyst can be ascribed to the fact that the immobilization procedure turns out, in spite of the extremely high surface to volume ratio, in an overall reduction of active surface area available for target molecule adsorption, due to the low porosity of the supported catalyst layer.

The kinetics of the investigated processes were monitored and a study on the reaction products and intermediates was carried out in order to evaluate possible difference in the reaction pathway in presence of immobilized nanoparticles versus suspended catalyst. The results demonstrate that the mechanisms of parent dye degradation in presence of supported TiO_2 nanoparticles are the same as those occurring in presence of TiO_2 Degussa P25 catalyst.

The present work describe the results obtained on the feasibility of scaling up the colloidal nanocrystal-based photocatalysis experiment: the comparison with a well standardized degradation method performed with a known material can allow a realistic evaluation of the advantages and the limits of the investigated nanoparticle towards the ultimate technology transfer.

Keywords: TiO_2 colloidal nanocrystals; TiO_2 Degussa P25; Degradation of organic dye; HPLC–MS; Photocatalysis

1. Introduction

In the area of water and wastewater treatments, advanced oxidation processes (AOPs) are well known for the ultimate removal of organic pollutants as a final cleaning step after conventional physicochemical or biological treatments, since AOPs are able to mineralize hazardous organic chemicals to carbon dioxide, water and simple mineral acids due to the efficient production of hydroxyl radicals ($^{\bullet}OH$), a powerful and non-selective oxidant specie [1–3].

In a photocatalytic process, the semiconductor is activated by ultraviolet (UV) radiation, establishing a redox environment in the aqueous solution, and thus acts as sensitizers for light-induced redox processes. TiO_2 is the most used photocatalyst due to its good performances, low cost and low toxicity. TiO_2 Degussa P25 is widely used in photocatalysis as a water suspension, even though other types of catalysts are commercially available [4,5]. However, the micrometric size of TiO_2 Degussa P25 particles, typically used in suspension, renders difficult to recover (and possibly recycle) them after water treatments. In fact, such drawback represents a severe limitation for scaling up the UV/TiO_2 process. As an alternative, several methods have been proposed to immobilize TiO_2 onto solid supports, such as fixed-bed reactors, in order to allow a continuous use of the

* Corresponding author. Tel.: +39 080 5820519; fax: +39 080 5313365.
E-mail address: giuseppe.mascolo@ba.irsa.cnr.it (G. Mascolo).

0304-3894/$ – see front matter © 2006 Elsevier B.V. All rights reserved.
doi:10.1016/j.jhazmat.2006.07.068

photocatalyst for processing of aqueous- or gas-phase effluents, without a post-process filtration step. In typical fixed-bed photocatalytic reactors, the photocatalyst is coated on the walls of the reactor [6], supported on a solid substrate or deposited around the case of the light source. Alternative supports have also been investigated, namely different types of glass, quartz, silica, activated carbon and zeolites [7]. Moreover, an effective entrapment of fine particles can be achieved by their immobilization on glass beads, on the walls of reaction vessels, on tube surface on glass or woven fibers, or they can be compressed into a ceramic membrane [7–9]. The fixation of TiO_2 on solid supports often reduces the efficiency of the photocatalytic process [4] as a consequence of a reduction in area of the active surface being a direct comparison of supported catalysts efficiency with respect to suspensions reported in some papers [4,10–12].

Nanostructured oxide crystals can be expected to compensate for the reduced performances associated with the immobilization process, that lead to a reduction in the active surface, by means of two main significant benefits deriving from the decrease in semiconductor particle size down to few nanometers [13–16]. The first derives from the extremely high surface-to-volume ratio typical of nanosized particles scales, consistent with a high surface density of active sites available for substrate adsorption, which makes it possible to increase the overall photoreaction rate. The second is due to the fact that when the semiconductor nanocrystal size is comparable or smaller than the bulk exciton diameter, the band gap becomes size-dependent due to quantization effects [17]. This allows the band gap to be tuned and, hence, also the electron–hole pair redox potentials. Consequently, a certain selectivity in the associated photoreactions can be achieved. A narrow size distribution is evidently fundamental in order to tailor the redox properties precisely as a function of crystal size. In addition, the presence of crystal defects, which can be associated to trap states for the photogenerated carriers, is generally poorer when high quality nanocrystals are accessible, thus allowing the electron–hole separation yield to be maximized [18]. All these characteristics can be achieved when TiO_2 nanocrystals are prepared by using colloidal chemical methods in coordinating solvents [15]. In addition, colloidal nanocrystals are characterized by a high processability that allow them to be easily deposited as prepared, or incorporated in a suitable nanocomposite, by using conventional deposition methods, such as spin coating, casting, etc.

In previous works [13–15], colloidal nanocrystalline TiO_2-based catalysts have been demonstrated to be more effective than commercial TiO_2 when tested in photodegradation experiments under the same experimental conditions. In the present paper, the comparison is carried out by testing the efficiency of TiO_2 Degussa P25 in aqueous suspension with that of the TiO_2 colloidal nanocrystals deposited onto the inner walls of a cylindrical photochemical reactor. This investigation was performed by using as model substrate an azo dye, methyl red (MR). The work was completed with the identification of the photodegradation by-products for the reactions monitored for the two photocatalytic systems, in order to evaluate possible diversity in the photocatalytic reaction mechanism.

2. Materials and methods

2.1. Chemicals

Titanium tetrachloride ($TiCl_4$, 99%), titanium isopropoxide (TTIP, 97%), *n*-heptadecane ($C_{17}H_{36}$ or HD, 99%), tri-*n*-octylphosphine oxide ($(C_8H_{17})_3PO$ or TOPO, 90%) and methyl red (2-(4-dimethylamino-phenylazo)-benzoic acid, C.I. 13020) (MR) were purchased from Aldrich. Commercial TiO_2 was TiO_2 "Degussa P25" (non-porous anatase; surface area, $50\,m^2\,g^{-1}$; mean diameter, approximately 30 nm). All solvents were HPLC grade and purchased from Fluka. Water used for liquid chromatography as well as for preparing all aqueous solutions (18.2 MΩ cm, organic carbon content $\leq 4\,\mu g/L$) was obtained from a Milli-Q Gradient A-10 system (Millipore).

2.2. Photocatalytic degradation

TiO_2 colloidal nanocrystals were prepared by exploiting a non-hydrolytic route, using standard air-free techniques, according to a procedure described in detail elsewhere [19]. Briefly, the synthesis was carried out by preparing two precursor stock solutions ($TiCl_4$, 1 M and TTIP, 1 M in HD) in a glove box. The $TiCl_4$ stock solution was injected in a three-neck flask kept under nitrogen flow containing a mixture of surfactants (TOPO and HD) previously degassed at 100 °C for 1 h under vacuum. Subsequently, the temperature was raised to 300 °C and the TTIP solution was injected, thus allowing the titanium dioxide to nucleate. After the TTIP injection, the temperature was lowered to 250 °C and the nanocrystal growth was completed in 10 min. The TOPO:Ti molar ratio in the starting reaction mixture is the key point to control the final nanocrystal size. TiO_2 nanocrystals were precipitated by adding an excess of MeOH and collected by centrifugation. The nanocrystals obtained were soluble in apolar solvents, such $CHCl_3$ or hexane, due to their non-polar surface coating (TOPO). The nanocrystals were deposited onto the inner walls of a cylindrical three-neck photo-reactor (275 mm high, 60 mm wide, with an available supporting area of approximately 500 cm^2) by rotary evaporating an optically clear $CHCl_3$ solution of organic-capped TiO_2 nanocrystals. The amount of the deposited catalyst was determined by mineralization of an aliquot of the $CHCl_3$ solution and following elemental quantitative analysis of the Ti, according to the procedure described below. Nanocrystalline TiO_2 was deposited on the inner wall of two identical reactors, covering the available surface with an amount of TiO_2 of 54 and 14 mg, respectively. The resulting film was thermally treated at 150 °C for 30 min to improve catalyst adhesion on the substrate. Although TOPO-capped TiO_2 deposited film is expected to be inherently stable due to the high resistance of the Ti–O–P bond toward hydrolysis and to the negligible solubility of TOPO in water, a reactor conditioning was performed on the supported catalyst in order to remove the surfactant layer, typically coordinated at the surface of the nanocrystals, as a consequence of the specific preparation route. For this purpose, the reactor with the supported catalyst was filled with water and exposed to prolonged UV treatment (about 10 h) monitoring, at scheduled times, the TOC of the solution.

It was found an initial TOC increase and then a reduction up to a value of about 1 mg/L that remained constant during prolonged exposure time. Similarly, in the experiments carried out on a TiO_2 Degussa P25 suspension, weighed amounts of catalyst were used in an identical type of reactor, as suspended catalyst.

A low pressure 17 W mercury lamp, emitting mainly at 254 nm, from Helios Italquartz (Italy) was used as radiating source. The reactors were typically filled with 500 mL of methyl red aqueous solution. the initial dye concentration was 4 mg L^{-1}. At scheduled irradiation times 5 mL of solution were withdrawn by means of a syringe. In the case of the experiment carried out on the suspended catalyst, a centrifugation step was necessary. All the samples were analyzed by means of high performance liquid chromatography-mass spectrometry (HPLC–MS). All experiments were performed under ambient atmosphere, keeping the system under vigorous stirring. The typical operative pH was adjusted to a value of 6, by adding an appropriate volume of HCl, 0.1 M solution.

2.3. Analytical determinations

The determination of residual dye concentration and by-product identification were performed by HPLC–UV–MS using a 1050-Ti chromatographic system equipped with a UV detector (Agilent), set at 220 nm, interfaced to an API 165 mass spectrometer (Applied Biosystem/MSD Sciex) by means of a turboionspray interface. Samples were injected by a Gilson 234 autosampler equipped with a 9010 Rheodyne valve and a 100 μL loop, and eluted at 1 mL/min through two Chromolith C18 columns (100 × 4.6 mm) in series and a Chromolith C18 pre-column (Merck) with the following gradient: from 70/25/5 (water/MeOH/50 mM AmAc in MeOH, pH 7) to 20/75/5 in 6 min, which was then maintained for 6 min. The MS interface conditions were as follows: needle voltage, 5000 V; declustering potential, 30 V; focusing potential, +200 V; mass range, 50–500 Th; scan time, 2 s; nebulizer gas flow (air), 1.5 L/min; curtain gas flow (nitrogen), 1 L/min; auxiliary gas flow (air) delivered by a turbo heated probe, 6 L/min at 300 °C. Injections were performed in duplicate and residual dye concentration values were obtained by a calibration curve. The flow from the HPLC–UV was split by means of a zero dead volume T-piece to allow about 200 μL/min to enter into the turboionspray interface.

Determination of dissolved Ti concentration was performed by inductively coupled plasma optical emission spectroscopy (ICP-OES) analysis using an Optima 3000 instrumentation (Perkin-Elmer).

3. Results and discussion

3.1. Characterization of nanostructured TiO_2

The nanocrystals, thus synthesized were then characterized by X-ray diffraction (XRD), transmission electron microscopy (TEM) and FT-IR spectroscopy. The peak positions in the XRD pattern (Fig. 1A) and their relative intensities could be exclusively indexed by the known standard TiO_2 anatase pattern

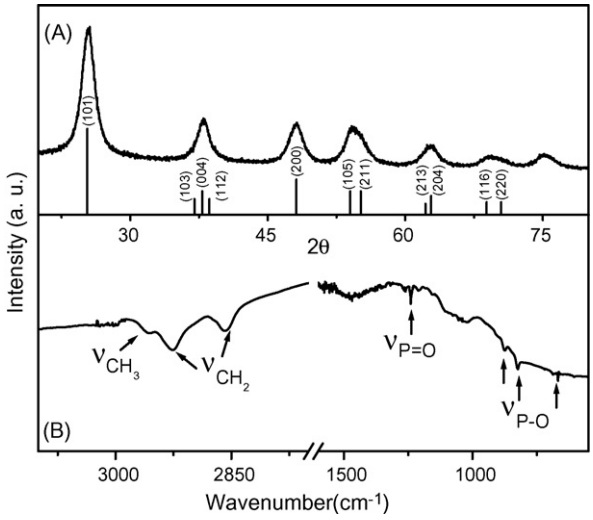

Fig. 1. (A) XRD pattern of TOPO-capped 6 nm TiO_2 nanocrystal powders. In the column diagram, the standard diffraction peaks of TiO_2 anatase are reported. (B) FT-IR spectra in the 3500–400 cm^{-1} region of TOPO-capped TiO_2 nanocrystals.

[15,19]. The average grain size was estimated to be about 6.0 nm by applying the Debye–Sherrer formula, demonstrating a good agreement with the mean particle size measured by transmission electron microscopy. Neither significant grain growth, nor phase transition was found to be induced by the moderate thermal treatment performed to improve the stability of the catalyst film. TEM images (data not shown) confirmed the nearly spherical morphology of the nanoparticles and their high degree of crystallinity [19].

As opposed to the TOPO-capped TiO_2 nanocrystal-based catalysts, the commercial TiO_2 Degussa P25 is composed of a mixture of the anatase (70%) and the rutile (30%) phases with a considerably larger mean particle size (mean diameter 33 nm) [20].

A comparison of the FT-IR spectra of the two types of catalysts was carried out in order to evaluate the characteristics of the chemical status of their surface. TiO_2 Degussa P25 present a FT-IR spectrum [21] characterized by the presence of a broad band around 3400 cm^{-1} and by a weak signal at 1650 cm^{-1} corresponding to the OH stretching and bending mode, respectively, both ascribable to the surface hydroxyl groups related to the adsorbed water (data not reported), thus confirming the organic-free surface of the TiO_2 Degussa P25.

The obtained spectrum of the as synthetized TiO_2 nanocrystals is reported in Fig. 1B. Above 2000 cm^{-1}, the intense peaks at about 2920 and 2850 cm^{-1}, respectively, can be ascribed with certainty to the antisymmetric and symmetric C–H stretching vibrations of the $–CH_2–$ groups in the hydrocarbon moiety. The shoulder visible at 2950–60 cm^{-1} can be associated to the asymmetric stretching of the terminal $–CH_3$ group of the alkyl chains. In the finger print region, a weak P=O stretching centered at about 1240 cm^{-1}, clearly detectable in pure TOPO, is still present in the spectrum of our TOPO-modified TiO_2 sample (Fig. 1B). In addition, the narrow bands ascribable to the P–O stretching at 1074, 1010 and 950 cm^{-1} in TOPO are remarkably broadened and shifted to lower wavenumbers. Below 950 cm^{-1},

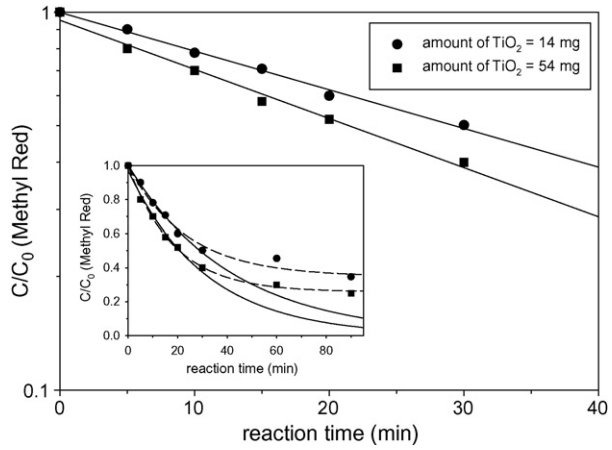

Fig. 2. Methyl red concentration decay during irradiation in the presence of deposited TiO_2 nanocrystals. The calculated first-order constants are reported in Table 1. In the inset graph are reported the residual methyl red concentrations also at reaction times higher than 30 min showing how: (i) they decrease more slowly than predicted considering first-order kinetics (full lines) and (ii) the fitting obtained using the equation $-dC/dt = k_1C - k_2(C_0 - C)$. Lamp input power 17 W, initial methyl red concentration 4 mg L^{-1}.

the characteristic vibrations of the inorganic Ti–O–Ti network in titanium dioxide can be seen.

The absence of the P=O stretching and the broadening of the P–O stretching bands has already been reported for ZrO_2 and TiO_2 surfaces modified with phosphonic [22–24] acids and interpreted as evidence of the coordination of all phosphoryl oxygens to surface Lewis acid sites and for the delocalization of electrons. Accordingly, the main bonding mode of phosphonate headgroups to the titania surface is known to involve both tridentate and bidentate attachments, thus accounting for the strong affinity of phosphonic acids for the TiO_2 surface.

3.2. Methyl red decay

MR concentration is plotted as a function of irradiation time during degradation with supported TiO_2 nanoparticles in Fig. 2. It is worth noting that MR decay is only due to photocatalysis as already published results showed practically no dye removal by UV radiation within 300 min [13]. In the early stage of the reaction (i.e. up to 30 min) MR degradation was found to follow first-order kinetics according to the equation $dC/dt = -kC$, where C is the MR concentration and k is the observed first-order rate constant. Instead, after a longer reaction time (inset of Fig. 2) MR concentration decreases more slowly than predicted considering first-order kinetics. This must have been due to the presence of by-products, which, once formed, being already very close to the TiO_2 nanoparticles must have actively competed with the parent compound for reaction with $^{\bullet}OH$ radicals. It is also possible, as proposed by Bayarri et al. [25], to use a kinetic equation that takes into account the influence of the first degradation products. Such a kinetic equation is:

$$-\frac{dC}{dt} = k_1C - k_2(C_0 - C)$$

where C_0 is the initial substrate concentration, C the substrate concentration, k_1 the kinetic constant of substrate decomposition and k_2 is the kinetic constant associated to by-product decomposition. This empirical equation, derived from common first-order kinetics, has been proposed for a simple description of the substrate decay and for scaling-up purposes although it is not really useful for mechanistic issues. However, it was found that the above reported equation is not suitable to account for the by-products influence. In fact, when fitting the experimental data (inset of Fig. 2) with the integrated form of the kinetic equation ($C = [C_0k_1/(k_1 + k_2)]\,e^{-(k_1+k_2)t} + [C_0k_2/(k_1 + k_2)]$), the obtained values of k_1 (0.028 and 0.040 for reactions with 14 and 54 mg of TiO_2 as absolute amount deposited, respectively) were significantly different from those obtained by fitting data of the early stage of the reaction (i.e. up to 30 min) with first-order equation (0.010 and 0.013 for reactions with 14 and 54 mg of TiO_2 loading, respectively).

Table 1
First-order constant (k) and half-life degradation times ($t_{1/2}$) of methyl red during photocatalytic reactions with immobilized TiO_2 nanoparticles and suspended TiO_2 Degussa P25

Absolute amount of catalyst (mg of TiO_2)	k (min^{-1})	$t_{1/2}$ (min)
14 (i)	0.010 ± 0.001	69 ± 7
54 (i)	0.013 ± 0.002	53 ± 8
14 (ii)	0.198 ± 0.018	3.5 ± 0.3
54 (ii)	0.190 ± 0.015	3.6 ± 0.3
500 (ii)	0.147 ± 0.011	4.7 ± 3

(i) indicates deposited; (ii) indicates suspended.

Furthermore, from Fig. 2 it is possible to note that the reaction rate is a function of the absolute TiO_2 amount deposited, since higher rates are found at higher TiO_2 loadings. However, on the basis of experimentally found k values (Table 1) it is evident that higher TiO_2 loadings do not produce a much higher MR removal rate (k increases from 0.010 to 0.013 min^{-1} by raising the TiO_2 loading from 14 to 54 mg) probably because the deposition procedure causes a multi-layer nanoparticle structure where the inner layers are not able to participate in the photocatalytic process.

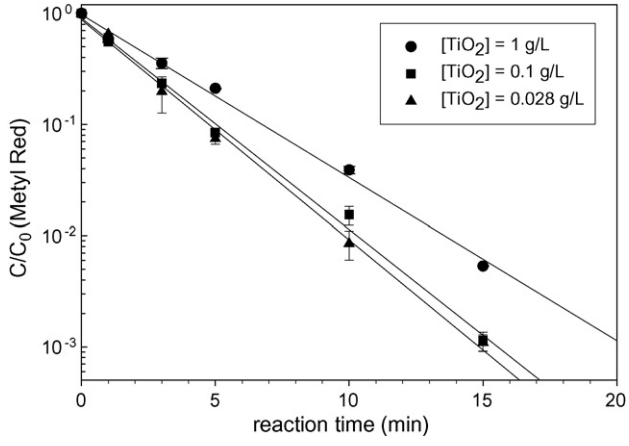

Fig. 3. Methyl red concentration decay during irradiation with suspended TiO_2 Degussa P25. The calculated first-order constants are reported in Table 1. Lamp input power 17 W, initial methyl red concentration 4 mg L^{-1}.

Fig. 3 shows MR concentration plotted as a function of irradiation time for the suspended TiO_2 catalyst. From this figure it is evident that the MR degradation reaction also follows a first-order kinetics for the suspended catalyst. In this case, for the investigated loading range (0.028–1 g/L), it was observed that the lower the TiO_2 concentration, the higher the degradation rate. Also, it was found that this trend reverted at catalyst concentrations lower than 0.01 g/L which, therefore, is the optimal catalyst concentration (highest MR degradation rate). The trend of Fig. 3 is similar to that reported for reactors having a capacity similar to that used in this study [26–28]. This result is, however, divergent from that found for photocatalytic oxidation of organic pollutants in smaller reactors where k increases at higher TiO_2 loadings before leveling-off at above 1 g/L [29–31]. It follows that the light penetration in the solution does affect the degradation process since the inner portion of the solution, closer to the light source, induces a scattering which is much more severe at higher titania content causing, in turn, a lack of absorption of the outer fraction of the solution.

A comparison of the MR degradation rate in presence of the two catalysts, respectively (Table 1), shows that the conventional TiO_2 Degussa catalyst, despite its higher particle dimensions, is more effective than the supported nanoparticles in the removal of the organic dye. In fact, the TiO_2 Degussa catalyzed a 50% dye abatement 20 times faster than the immobilized TiO_2 at 14 mg absolute loading, requiring 3.5 instead of 69 min. Again, at 54 mg TiO_2 loading, the same dye abatement was 15 times faster with the TiO_2 Degussa catalyst (3.6 with respect to 53 min). The poorer performance of the nanoparticle-based catalyst can be ascribed to the fact that the immobilization process is known to reduce intrinsically the active surface area available for adsorption and catalysis through the formation of several non-porous layers. It follows that only a fraction of the overall surface of the nanocrystals is available for the photocatalytic process. The extent of this fraction is strongly influenced by the degree of porosity and permeability of the deposited film of nanocrystals. Under the investigated experimental conditions the amount of active sites available on the immobilized nanosized

Table 2
Chemical structures and main fragment ion masses of methyl red and by-products identified during photocatalytic degradation with immobilized TiO_2 nanoparticles and suspended TiO_2 Degussa P25

By-product	Chemical structure	Molecular weight	Retention time (min)	$[M+H]^+$ and main fragment ion masses (relative intensity)	P25-TiO_2	Immobilized nano-TiO_2
Methyl Red	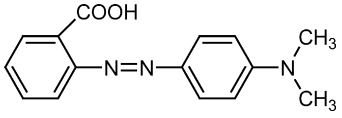	269	7.2	270 (100), 252 (72), 224 (6), 209 (8), 196 (7)	–	–
1	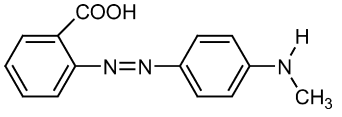	255	6.2	256 (100), 238 (89), 210 (10), 196 (12),	X	X
2	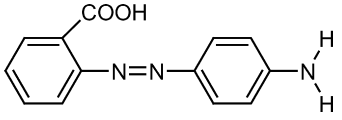	241	4.6	242 (100), 224 (99), 196 (20)	X	X
3,3′ (2 isomers)	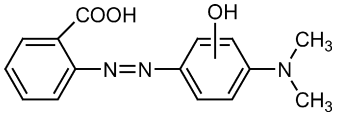	285	6.6, 7	286 (100), 268 (50), 240 (5)	X	X
4,4′ (2 isomers)	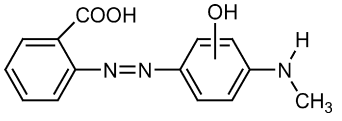	271	5.4, 6.1	272 (100), 254 (97), 226 (9)	X	X
5	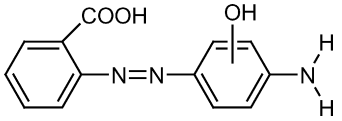	257	3.6	258 (100), 240 (98), 212 (7)	X	X
6	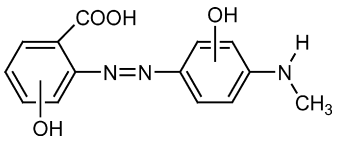	287	6.4	288 (100), 270 (80)	X	

catalyst is apparently smaller than that accessible on the equivalent suspended counterpart, as evidenced by the efficiency rates obtained in the experiment reported. However, the nanoparticle-based catalyst proved to be quite stable during the UV tests as demonstrated by the fact that after the degradation procedure, the dissolved Ti concentration was always found below 50 μg/L.

3.3. By-product formation

By-product formation was investigated by performing HPLC–MS analysis on irradiated reaction mixtures in order to compare the reaction course for the immobilized nanoparticle catalyst and the suspended commercial TiO_2. Table 2 reports the chemical structures of MR and the main by-products identified during degradation reaction by using TiO_2 Degussa P25 and immobilized TiO_2 nanoparticles as catalyst, respectively, and highlights that no evident difference can be inferred for the two investigated systems. The identification of the by-products was accomplished by interpreting the main fragment ions of their mass spectra (Table 2). The mass spectra of all by-products showed a fragmentation pathway similar to that of MR reported in Fig. 4. In particular, the $[M+H]^+$ ion and that deriving from water loss always showed to be the base peaks. Minor ions were found corresponding to subsequent CO elimination from the latter ion and deriving from further methyl and ethylene loss. Obviously, the latter fragmentation is only possible for by-products keeping the *N*-dimethyl moiety. It is worth noting that all by-products were identified in positive ion mode but also HPLC–MS analyses in negative ion mode were carried out in order to detect any phenolic compounds. However, no by-products were detected in negative ion mode. The experimental data obtained are consistent with the occurrence of two different mechanisms of degradation of the parent compound. The first mechanism is due to $O_2^{\bullet -}$ generated by O_2 reduction by free photoelectrons in the conduction band of catalyst and to the formation of hydroxyl radicals originating either from the oxidation of OH^- or H_2O by the photogenerated holes [2]. It gives rise to the oxidation of methyl group leading to the formation of by-product 1. This route can also be followed, consecutively, by oxidation of the second methyl group leading to by-product 2. The

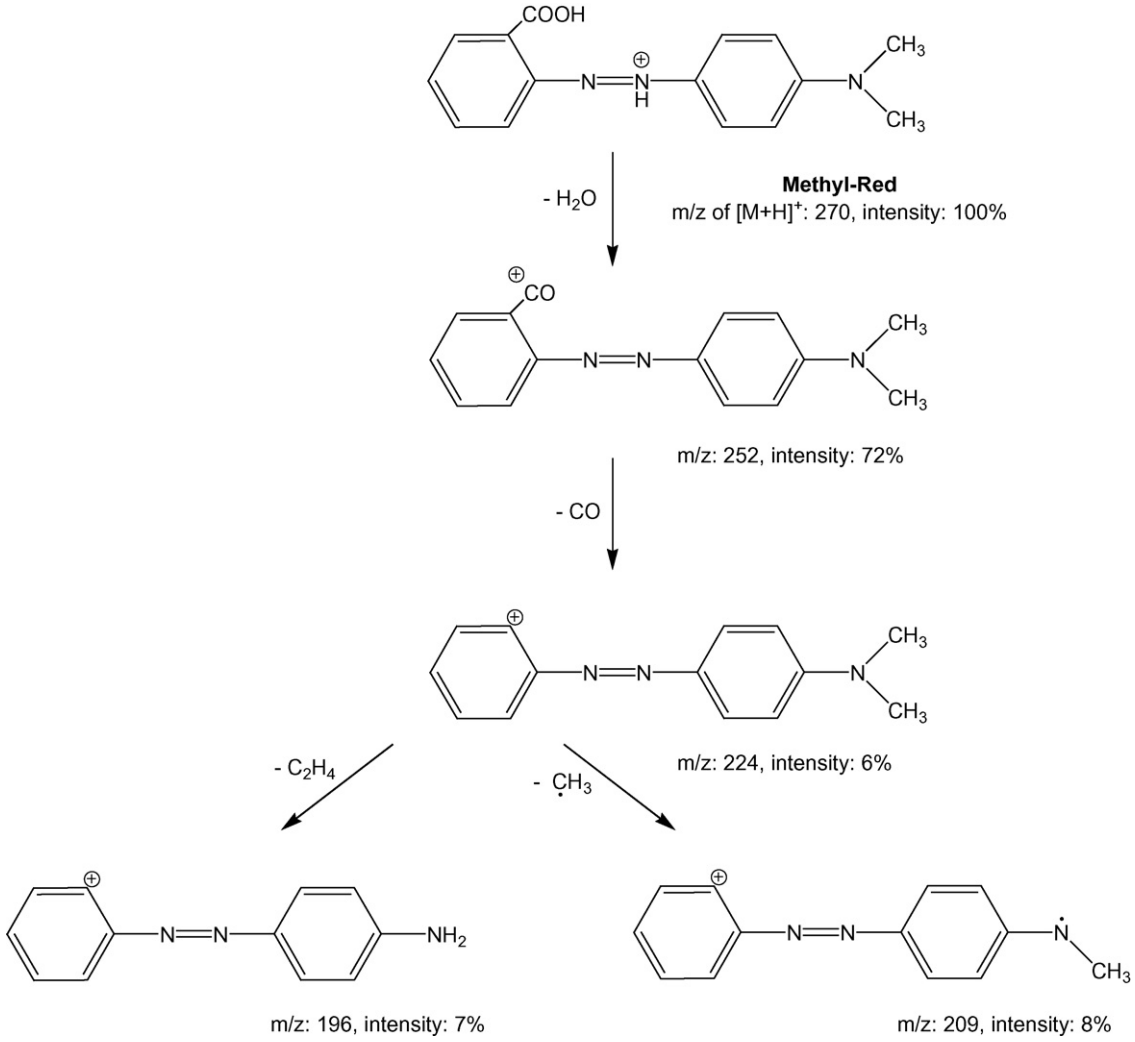

Fig. 4. Proposed fragmentation pathway of methyl red from LC/MS analysis.

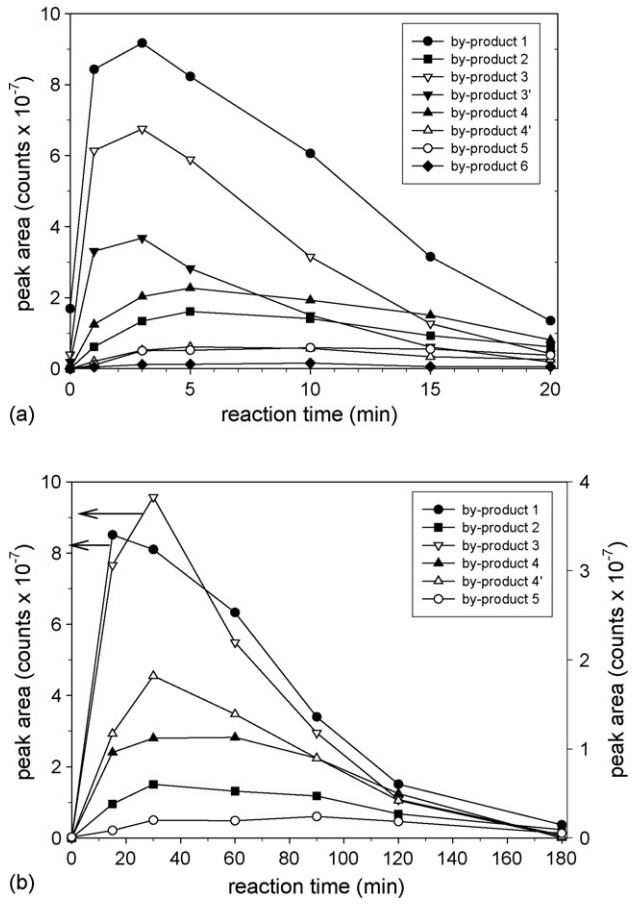

Fig. 5. Evolution profiles of identified by-products during methyl red degradation with suspended P25 Degussa TiO_2 (a) and immobilized TiO_2 nanoparticles (b).

second mechanism is only based on the formation of hydroxyl radicals that, in turn, can react with the parent dye by addition to the aromatic rings leading to hydroxylated by-product 3. The two mechanisms can be operative independently, as proven by the presence of by-products 4 and 5. Also, the hydroxyl radical addition can occur consecutively leading to the formation of the poly-hydroxylated by-product 6. This by-product was not detected for the experiments performed using immobilized nanoparticles as catalyst. Probably its absence in the by-product pattern can be due to its formation in very small amounts, probably below the instrumentation detection limit. In fact, even during the reaction catalyzed by the Degussa TiO_2, the smallest peak area (Fig. 5) in the overall chromatogram was that associated to by-product 6, thus evidencing a low yield. It is also important to note that OH substitution probably occurs on the benzene ring carrying the dimethylamino group, since it is able to stabilize the intermediate hydroxy-benzene radical, unlike the other benzene ring which carries the electron withdrawing COOH moiety. In addition, for some by-products two isomers were identified as expected on the basis of the non-selective mode of hydroxyl radical reactions.

In Fig. 5, the temporal evolution profiles of identified by-products during degradation with the investigated catalysts are reported. All profiles show a maximum of intermediate byproduct formation at reaction times between 3–5 and 2–40 min during the treatment with TiO_2 Degussa P25 and immobilized TiO_2 nanoparticles, respectively. These findings are consistent with the MR decay plots (Fig. 2) showing the higher removal rate of TiO_2 Degussa P25 catalyst with respect to supported TiO_2 nanoparticles. However, it is worthwhile to highlight that the reported trends should be considered semi quantitative, due to the lack of standards for the identified by-products. Fig. 5 also displays for both catalysts the disappearance of all by-products at prolonged reaction times (higher than 20 and 180 min for reactions with the TiO_2 Degussa P25 catalyst and with the supported nanoparticles, respectively). At such long reaction times no by-products were detected during HPLC–MS analyses and the reaction mixtures appeared to be colorless. Such behavior is consistent with the opening of the dye aromatic rings and with the azo-bond breakdown, due to the consecutive $^{\bullet}OH$ radical attack, which ultimately lead to the formation of low molecular weight compounds (organic acids) not detectable by HPLC–MS. Such end by-products are expected to be polar and to exhibit a lower affinity for TiO_2, the latter behavior not being a real problem since they are not toxic compounds.

4. Conclusion

The photocatalytic efficiency of supported TiO_2 colloidal nanocrystals, immobilized onto a glass substrate was compared to commercial TiO_2 Degussa P25 catalyst, by using as model compound the azo dye MR. Experimental results showed that:

- the conventional TiO_2 Degussa P25 catalyst, despite its higher particle dimensions was more effective than the supported TiO_2 nanoparticles in the MR removal process;
- the limited photocatalytic efficiency of the nanoparticle-based system can be ascribed to the fact that the immobilization process reduces the active surface area available for adsorption and catalysis;
- the mechanisms for parent dye degradation reaction in presence of either of immobilized nanoparticles and suspended catalyst were the same.

Finally, it is worthwhile to note that an enhancement of the performance of the nanoparticle-based catalyst could be obtained by optimizing the deposition procedures in order to achieve an highly porous nanocrystal-based film, able to overcome the drawbacks deriving from the lost in active area due to immobilization. Further studies are also in progress to test different deposition techniques and to test the effect of nanoparticle shape on the photocatalytic processes.

Acknowledgements

This work was partially supported by Progetto MIUR D.M. no. 1105 (9 October 2002) funding programme. INSTM (Italy) is also gratefully acknowledged.

References

[1] R. Andreozzi, V. Caprio, A. Insola, R. Marotta, Advanced oxidation processes (AOP) for water purification and recovery, Catal. Today 53 (1999) 51–59.

[2] J.M. Hermann, Heterogeneous photocatalysis: state of the art and present applications, Top. Catal. 34 (2005) 49–65.

[3] O. Prieto, J. Fermoso, Y. Nuñez, J.L. del Valle, R. Irusta, Decolouration of textile dyes in wastewaters by photocatalysis with TiO_2, Sol. Energy 79 (2005) 376–383.

[4] A. Rachel, M. Subrahmanyam, P. Boule, Comparison of photocatalytic efficiencies of TiO_2 in suspended and immobilised form for the photocatalytic degradation of nitrobenzenesulfonic acids, Appl. Catal. B: Environ. 37 (2002) 301–308.

[5] C. Guillard, H. Lachheb, A. Houas, M. Ksibi, E. Elaloui, J.-M. Herrmann, Influence of chemical structure of dyes, of pH and of inorganic salts on their photocatalytic degradation by TiO_2 comparison of the efficiency of powder and supported TiO_2, J. Photochem. Photobiol. A 158 (2003) 27–36.

[6] D.W. Bahnemann, D. Bockelmann, R. Goslich, R.M. Hilgendor Weichgrebe, in: D.W. Ollis, H. Al-Ekabi (Eds.), Photocatalytic Purification and Treatment of Water and Air, Elsevier, Amsterdam, 1993, pp. 301–319.

[7] R.L. Pozo, M.A. Baltanás, A.E. Cassano, Supported titanium oxide as photocatalyst in water decontamination: state of the art, Catal. Today 39 (1997) 219–231 (and references therein).

[8] A. Karim, J. Bravo, D. Gorm, T. Conant, A. Datye, Comparison of wall-coated and packed-bed reactors for steam reforming of methanol, Catal. Today 110 (2005) 86–91.

[9] K.L. Yeung, X. Zhang, W.N. Lau, R. Martin-Aranda, Experiments and modeling of membrane microreactors, Catal. Today 110 (2005) 26–37.

[10] A. Fernández, G. Lassaletta, V.M. Jiménez, A. Justo, A.R. González-Elipe, J.-M. Herrmann, H. Tahiri, Y. Ait-Ichou, Preparation and characterization of TiO_2 photocatalysts supported on various rigid supports (glass, quartz and stainless steel). Comparative studies of photocatalytic activity in water purification, Appl. Catal. B: Environ. 7 (1995) 49–63.

[11] V.A. Sakkas, I.M. Arabatzis, I.K. Konstantinou, A.D. Dimoua, T.A. Albanis, P. Falaras, Metolachlor photocatalytic degradation using TiO_2 photocatalysts, Appl. Catal. B: Environ. 49 (2004) 195–205.

[12] S. Parra, S.E. Stanca, I. Guasaquillo, K.R. Thampi, Photocatalytic degradation of atrazine using suspended and supported TiO_2, Appl. Catal. B: Environ. 51 (2004) 107–116.

[13] M.L. Curri, R. Comparelli, P.D. Cozzoli, G. Mascolo, A. Agostiano, Colloidal oxide nanoparticles for the photocatalytic degradation of organic dye, Mater. Sci. Eng. C: Bio. S. 23 (2003) 285–289.

[14] R. Comparelli, E. Fanizza, M.L. Curri, P.D. Cozzoli, G. Mascolo, R. Passino, A. Agostiano, Photocatalytic degradation of azo dyes by organic-capped anatase TiO_2 nanocrystals immobilized onto substrates, Appl. Catal. B: Environ. 55 (2005) 81–91.

[15] R. Comparelli, P.D. Cozzoli, M.L. Curri, A. Agostiano, G. Mascolo, G. Lovecchio, Photocatalytic degradation of methyl red by immobilised nanoparticles of TiO_2 and ZnO, Water Sci. Technol. 49 (2004) 183–188.

[16] R. Comparelli, E. Fanizza, M.L. Curri, P.D. Cozzoli, G. Mascolo, A. Agostiano, UV-induced photocatalytic degradation of azo dyes by organic-capped ZnO nanocrystals immobilized onto substrates, Appl. Catal. B: Environ. 60 (2005) 1–11.

[17] C.N.R. Rao, G.U. Kulkarni, P.J. Thomas, P.P. Edwards, Size-dependent chemistry: properties of nanocrystals, size-dependent chemistry: properties of nanocrystals, Chem. Eur. J. 8 (2002) 28–35.

[18] R. Amal, S. McEvoy, D. Beydoun, G. Low, Role of Nanoparticles in Photocatalysis, J. Nanopart. Res. 1 (1999) 439–458.

[19] T.J. Trentler, T.E. Denler, J.F. Bertone, A. Agrawal, V.L. Colvin, Synthesis of TiO_2 nanocrystals by non-hydrolytic solution-based reactions, J. Am. Chem. Soc. 121 (1999) 1613–1614.

[20] A.K. Datye, G. Riegel, J.R. Bolton, M. Huang, M.R. Prairie, Microstructural characterization of a fumed titanium dioxide photocatalyst, J. Solid State Chem. 115 (1995) 236.

[21] Z. Ding, G.Q. Lu, P.F. Greenfield, Role of the crystallite phase of TiO_2 in heterogeneous photocatalysis for phenol oxidation in water, J. Phys. Chem. B 104 (2000) 4815–4820.

[22] J. Thistlewaite, M.S. Hook, Diffuse reflectance Fourier transform infrared study of the adsorption of oleate/oleic acid onto titania, Langmuir 16 (2000) 4993–4998.

[23] J. Thistlewaite, M.L. Gee, D. Wilson, Diffuse reflectance infrared Fourier transform spectroscopic studies of the adsorption of oleate/oleic acid onto zirconia, Langmuir 12 (1996) 6487–6491.

[24] M. Nara, H. Tori, M. Tasumi, Correlation between the vibrational frequencies of the carboxylate group and the types of its coordination to a metal ion: an ab initio molecular orbital study, J. Phys. Chem. 100 (1996) 19812–19817.

[25] B. Bayarri, J. Gimenez, D. Curco, S. Esplugas, Photocatalytic degradation of 2,4-dichlorophenol by TiO_2/UV: kinetics, actinometries and models, Catal. Today 101 (2005) 227–236.

[26] J.H. Lee, W. Nam, M. Kang, G.Y. Han, K.J. Yoon, M.-S. Kim, K. Ogino, S. Miyata, S.-J. Choung, Design of two types of fluidized photo reactors and their photo-catalytic performances for degradation of methyl orange, Appl. Catal. A: Gen. 244 (2003) 49–57.

[27] N. Daneshvar, D. Salari, A.R. Khataee, Photocatalytic degradation of azo dye acid red 14 in water: investigation of the effect of operational parameters, J. Photochem. Photobiol. A 157 (2003) 111–116.

[28] M.S.T. Gonçalves, A.M.F. Oliveira-Campos, E.M.M.S. Pinto, P.M.S. Plasencia, M.J.R.P. Queiroz, Photochemical treatment of solutions of azo dyes containing TiO_2, Chemosphere 39 (1999) 781–786.

[29] R. Andreozzi, V. Caprio, A. Insola, G. Longo, V. Tufano, Photocatalytic oxidation of 4-nitrophenol in aqueous TiO_2 slurries: an experimental validation of literature kinetic models, J. Chem. Technol. Biotechnol. 75 (2000) 131–136.

[30] N. San, A. Hatipoglu, G. Kocturk, Z. Cinar, Photocatalytic degradation of 4-nitrophenol in aqueous TiO_2 suspensions: theoretical prediction of the intermediates, J. Photochem. Photobiol. A 146 (2001) 189–197.

[31] K. Chiang, R. Amal, T. Tran, Photocatalytic oxidation of cyanide: kinetic and mechanistic studies, J. Mol. Catal. A 193 (2003) 285–297.